A Model-Based Approach to Reach a 3D Target with a Soccer Ball, Kicked by a Soccer Robot

Jordy Senden, Yanick Douven and René van de Molengraft
Department of Mechanical Engineering
Eindhoven University of Technology
Eindhoven, The Netherlands

***Abstract*—This paper describes an approach to reach a specified, three dimensional target with a soccer ball, potentially with intermediate bounces, using a soccer robot as used in the RoboCup Middle Size League. A model of a freely moving, bouncing ball is created and validated. From this model the initial ball states to achieve a desired target can be calculated. Next, the interaction between the robot and the ball is modelled, which predicts the initial ball state for certain inputs to the robot. In this interaction model the ball is modelled as a mass-spring-damper system. In addition, this paper proposes a theoretical correlation between the coefficient of restitution, commonly used to account for energy losses after impact, and the mass-spring-damper system. The interaction model is used to find a static mapping between the robot inputs and initial ball state. This map is used to choose the correct inputs leading to the desired initial ball state. To verify the presented method, the soccer robots of team Tech United Eindhoven are used to shoot at several targets. With the presented method the impact position of the ball can be predicted with an accuracy lower than the ball diameter.**

I. Introduction

RoboCup[1] is an international initiative to promote and advance research in robotics and artificial intelligence. Founded in 1997, its main goal is to 'develop a team of fully autonomous humanoid robot soccer players which is able to win against the winner of the most recent World Cup, complying with the official rules of FIFA, by the middle of the 21st century'. In the Middle Size League (MSL), two teams of five autonomous robots play a soccer match on an artificial field. The soccer robots of Tech United are named TURTLEs, which is an acronym for Tech United RoboCup Team Limited Edition. These robots are able to drive around while using several on-board camera's to position themselves on the field. Moreover, they can determine the position of the ball, opponents and team mates. Through radio signals they can communicate with each other and decide upon a strategy. With a ball-handling system the ball can be captured and controlled and a shooting mechanism is able to shoot a ball over the ground or through the air. The goal of this research is to enable the TURTLEs to shoot the ball through the air, to hit a predefined target, based on models of a freely flying ball and robot-ball interaction.

Many research that has been done on the flight of a ball concentrates on the aerodynamics, such as [1]–[3]. This is not yet relevant in robot soccer, since the speed of the ball is not high enough for aerodynamic forces to have a significant influence on the path of the ball [1]. The bounce of a ball is broadly investigated, for example by Cross [4]–[8], which is used as a start to develop the theory in Section II. Less research has been done on controlling a robotic actuator in order to aim a ball at a target. In [9] the ball is shot with a robotic leg and in [10] a humanoid robot is used to shoot the ball. Both also disregard aerodynamic effects as a first estimate, but do not incorporate an intermediate bounce. The approach of modelling the impact dynamics between the kicker and ball is similar to the approach taken in this research. In [11] both the flight, including aerodynamics, and the bounce of a table tennis ball is discussed, without making an effort to estimate the desired inputs to aim the ball at a target. This paper will deal with determining the desired initial state of a standard soccer ball, to make its trajectory pass through a target, and how to enforce this state with the robot by determining the correct robot inputs. The goal is to be able to hit a target with an accuracy of at least one times the ball diameter.

In Section II the motion of a freely moving ball is discussed, where the flight dynamics and the bounce are presented and tested. Section III discusses the model which describes the interaction between the TURTLE and the ball. In Section IV this model is used to determine the correct settings for the robot. In Section V experiments are discussed to test the models and the results are discussed. In Section VI conclusions are drawn from the results of the experiments and recommendations are made for future work.

II. Free Ball Motion

The objective of 'aiming a ball' is to give the ball an appropriate initial state, such that its travelled path will pass through a predefined three dimensional point in space, i.e. the target. In order to do this successfully, the path of the ball should be predictable for any given initial state. The path of a bouncing ball can be divided into two recurring phases; a free flight followed by a bounce on the floor. Both phases have different dynamics and thus a different effect on the states of the ball, which will be explained in this section.

[1] http://www.robocup.org/

A. Free Flight

When a ball moves through the air with a certain velocity, it will experience several forces, as illustrated in Fig. 1. The gravitational force is directed towards the ground and a drag force, caused by aerodynamic effects, is directed in opposite direction of the ball's velocity. When the ball is also spinning, it will experience a force that is caused by the Magnus effect and is directed orthogonal to the velocity and spin vector [1]. When the ball possesses sidespin, this Magnus force is able to force the ball out of its vertical plane of motion and thus give it 'effect'.

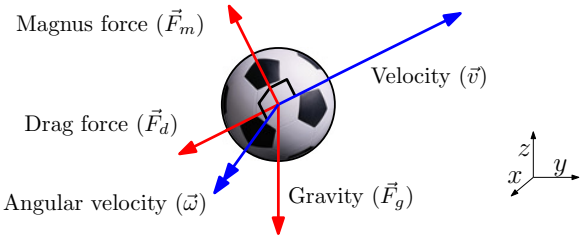

Fig. 1: An example of forces acting on a flying ball with a linear and angular velocity. In this example the ball possesses back spin. Since the Magnus force is perpendicular to both the linear and angular velocity vectors it creates a lift force in this case.

At low velocities and spin values, the gravitational force will have the biggest influence on the ball. In [1] it is shown that the drag- and Magnus force on a soccer ball is only of significant influence at velocities larger than 20 ms^{-1} and spin ratios of order 0.02 or higher. The spin ratio is defined as $R_b\omega_0 v_0^{-1}$, with R_b the radius of the ball and ω_0 and v_0 the initial angular and linear velocity of the ball respectively. The TURTLEs can shoot a ball with a maximal absolute velocity of approximately 12 ms^{-1}, therefore the drag force can be neglected. Since the radius of a standard soccer ball is approximately 0.11 m, the ball should have an angular velocity of about 4.5π radians per second at its maximal velocity for the Magnus force to become significant. The model discussed in Section III will show this can not be achieved with the current set up. Therefore, aerodynamic effects are omitted and the motion of the ball, while in free flight, can be described by the linear state space equation:

$$\dot{\boldsymbol{q}} = [v_x, v_y, v_z, 0, 0, -g, 0, 0, 0]^T \tag{1}$$

where the state vector, $\boldsymbol{q} = [x, y, z, v_x, v_y, v_z, \omega_x, \omega_y, \omega_z]^T$, contains the balls position and linear- and angular velocity components in three directions and g represents the gravitational acceleration. . This system is described with respect to a right handed Cartesian coordinate system. The origin of this system is set at the centre of the robot, with its z-axis normal to the surface of the soccer field and its y-axis pointing in the direction of the robot heading.

B. Bounce of a Spinning Ball

After its flight the ball will hit the ground, in this case the artificial soccer field, which is assumed to be infinitely stiff relative to the ball. This means that the field surface stays fixed at impact, while the ball deforms. Not all energy is conserved during impact, some is lost due to friction in the shell material of the ball during deformation [12]. This loss of energy prevents the ball from reaching its initial height, when dropped vertically to the ground. In vertical direction, the velocity component of the ball after impact (v_z^+) is lower than before the impact (v_z^-). This energy loss can be captured by a coefficient of restitution (COR), which is defined as

$$\epsilon_z = -\frac{v_z^+}{v_z^-} = \sqrt{\frac{h^+}{h^-}} \tag{2}$$

where ϵ_z is the COR, h^+ the dropping height and h^- the maximum height the ball reaches after the bounce [13]. The COR depends on ball properties, such as material, inner pressure and orientation during the bounce, as well as on the surface it bounces from. If the impact velocity is known, the vertical velocity component of the ball after the impact can be calculated using (2).

In horizontal direction, if the friction between the ball and the surface is heigh enough, there is a correlation between the horizontal velocity component and the spin of the ball during impact. One can imagine a ball without spin hitting the field surface under an oblique angle. After bouncing, this ball will have developed spin. Moreover, a spinning ball falling vertically to the floor will bounce sideways, provided the angular velocity vector has a component in the direction of the plane. This correlation can be explained by looking at the contact point between the ball and the surface at the time of impact. From Fig. 2 it can be seen that the velocity of the contact point may differ from the velocity of the centre of gravity of the ball, when the ball has an angular velocity. In the figure, $\vec{v}_G$ and $\vec{\omega}_G$ represent the linear and angular velocity with respect to the centre of gravity of the ball. When the velocity of the contact point in horizontal direction differs from the velocity of the surface of the floor, which is assumed to be zero, friction between the surface of the ball and the floor will cause a tangential force on the ball.

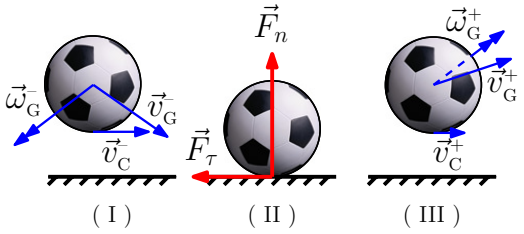

Fig. 2: An example of a bouncing ball split up into three parts: just before the ball hits the surface (I), the point at which $v_{G,z} = 0$ (II) and just after the ball looses contact with the surface (III). In this example, the ball possesses backspin before the impact with the floor.

The velocity and spin after a bounce can be estimated by solving a force- and momentum equilibrium during the impact. In [6] a similar approach is explained for a two dimensional problem. Two external forces acting on the ball

during the bounce are the normal force $\vec{F}_n$ and a tangential force $\vec{F}_\tau$. The start and end of the bounce occur at t^- and t^+ respectively. During the entire contact time a force and momentum equilibrium in all three directions should hold. Integrating force and momentum over the impact time results in an expression for the linear and angular impulse:

$$\int_{t^-}^{t^+} F_i dt = m \int_{t^-}^{t^+} \dot{v}_i dt = m\big(v_i^+ - v_i^-\big) \tag{3}$$

$$\int_{t^-}^{t^+} M_i dt = I_G \int_{t^-}^{t^+} \dot{\omega}_i dt = I_G\big(\omega_i^+ - \omega_i^-\big) \tag{4}$$

where m is the mass of the ball, I_G its mass moment of inertia and F_i, $\dot{v}_i$, M_i and $\dot{\omega}_i$ represent the force, linear acceleration, momentum, and angular acceleration in the i-direction ($i \in \{x, y, z\}$), with respect to the centre of the ball, respectively. The rotation of the ball is described with respect to its centre of gravity, therefore the mass moment of inertia of the ball is the same in all three directions and can be calculated as $I_G = \alpha m R_b^2$. Where α is a factor which accounts for the shell thickness of the ball and the indentation of the ball during the bounce. For a solid sphere $\alpha = \frac{2}{5}$ and for a thin spherical shell $\alpha = \frac{2}{3}$. A soccer ball resembles a spherical shell with a certain shell thickness, therefore its α should be of the same order. During the bounce the ball will deform, which causes the radius of the ball to become smaller for a short period. Since R_b is assumed constant, this short decrease in radius can be captured by increasing α. The factor α is a ball property and is determined from measurements. There is only one force working in the principle directions. The momentum around the centre of the ball is created by the tangential force only:

$$\int_{t^-}^{t^+} M_x dt = R_b \int_{t^-}^{t^+} F_{\tau,y} dt \tag{5}$$

$$\int_{t^-}^{t^+} M_y dt = -R_b \int_{t^-}^{t^+} F_{\tau,x} dt \tag{6}$$

Combining (3) - (6) and using the expression for the mass moment of inertia of a ball gives:

$$\alpha m R_b^2(\omega_x^+ - \omega_x^-) = R_b m(v_y^+ - v_y^-) \tag{7}$$

$$\alpha m R_b^2(\omega_y^+ - \omega_y^-) = -R_b m(v_x^+ - v_x^-) \tag{8}$$

The momentum around the z-axis is equal to zero, since the ball is assumed to be perfectly spherical and the contact point infinitely small. This would mean that a ball with spin around its z-axis will never loose this spin. In reality the contact point will not be infinitely small but will be a surface, especially when impacting at high velocities [12]. Due to this, friction forces can result in a minor loss of spin in z-direction. Analogous to (2), the spin around the z-axis is estimated by

$$\omega_z^+ = \varepsilon_z(v_z)\omega_z^- \tag{9}$$

where $\varepsilon_z(v_z)$ can be seen as a COR for rotation around the z-axis. This spin has no influence on the net friction force, and thus on the path of the ball. It is therefore not necessary to elaborate on $\varepsilon_z(v_z)$ in order to predict the path of the ball. It is assumed that the friction between the ball and the surface of the floor is high enough and that the ball will not slip. When the ball leaves the surface, the velocity of the contact point tangential to the surface will be zero:

$$v_{C,x}^+ = v_x^+ - R_b\omega_y^+ = 0 \tag{10}$$

$$v_{C,y}^+ = v_y^+ + R_b\omega_x^+ = 0 \tag{11}$$

where $v_{C,x}$ and $v_{C,y}$ are the velocity components of the contact point in x- and y-direction respectively. Using (10) and (11), in combination with (7) and (8), and (2) and (9), the state of the ball after the bounce ($\boldsymbol{q}^+$) can be predicted as a function of the state before the impact ($\boldsymbol{q}^-$).

$$\boldsymbol{q}^+ = \boldsymbol{B}\boldsymbol{q}^- \tag{12}$$

where $\boldsymbol{B}$ is the state transition matrix for the discrete time event of the bounce:

$$\boldsymbol{B} = \begin{bmatrix} \boldsymbol{I}_{3\times3} & \boldsymbol{O}_{3\times6} \\ \boldsymbol{O}_{6\times3} & \boldsymbol{T}_{6\times6} \end{bmatrix} \tag{13}$$

with

$$\boldsymbol{T} = \begin{bmatrix} \frac{1}{\alpha+1} & 0 & 0 & 0 & \frac{\alpha R_b}{\alpha+1} & 0 \\ 0 & \frac{1}{\alpha+1} & 0 & \frac{-\alpha R_b}{\alpha+1} & 0 & 0 \\ 0 & 0 & -\epsilon_z & 0 & 0 & 0 \\ 0 & \frac{-1}{R_b(\alpha+1)} & 0 & \frac{\alpha}{\alpha+1} & 0 & 0 \\ \frac{1}{R_b(\alpha+1)} & 0 & 0 & 0 & \frac{\alpha}{\alpha+1} & 0 \\ 0 & 0 & 0 & 0 & 0 & \varepsilon_z \end{bmatrix}. \tag{14}$$

C. Full Path of a Freely Bouncing Ball

The motion of a bouncing ball can be described by a hybrid system, as described in [14], where the continuous dynamics of the flight is followed by the discrete time event of the bounce. In Fig. 3 a representation of the system is shown. The initial state of the ball ($\boldsymbol{q}_0$) should exist in the set of all possible initial states ($Init$). If the ball is in the air ($z \geq R_b$), its motion is described by (1). When the ball hits the surface, i.e. when the guard (G) hold, a discrete state transition occurs according to (12). Using this model, the path of the ball can be calculated up to an arbitrary number of bounces, given an initial state vector.

The position of the ball as a function of time can be found by solving the equations of motion of the flight (1):

$$x(\tau) = v_{x,\tau_0}\tau + x_{\tau_0} \tag{15a}$$

$$y(\tau) = v_{y,\tau_0}\tau + y_{\tau_0} \tag{15b}$$

$$z(\tau) = v_{z,\tau_0}\tau - \tfrac{1}{2}g\tau^2 \tag{15c}$$

$$\tau(t) = t - t_{b,k} \tag{15d}$$

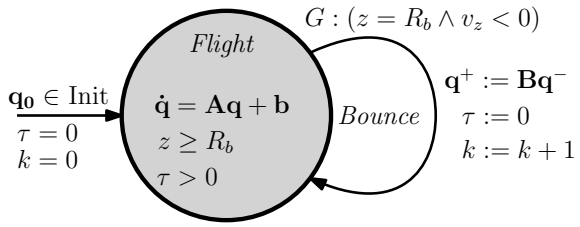

Fig. 3: The dynamics of a bouncing ball represented as a hybrid automaton.

where τ is a time parameter which is reset to 0 after every bounce and $t_{b,k}$ is the actual time of the k^{th} bounce. Setting $k = 0$ gives the initial position, velocity and time of the ball when it is kicked. The last bounce location depends on all previous bounce locations and velocity components. Each bounce location can be solved by recursively solving $z(\tau) = 0$ in (15c), solving for τ and using this τ in (15a) and (15b), which results in:

$$\begin{aligned} x(\tau,k) &= v_{x,\tau_0}\tau + \frac{2v_{z,0}}{g}\sum_{i=1}^{k} v_{x,t_{b,k-i}}\epsilon_z^{k-i} \\ y(\tau,k) &= v_{y,\tau_0}\tau + \frac{2v_{z,0}}{g}\sum_{i=1}^{k} v_{y,t_{b,k-i}}\epsilon_z^{k-i} \\ z(\tau,k) &= v_{z,0}\epsilon_z^k\tau - \tfrac{1}{2}g\tau^2 \\ \tau(t,k) &= t - \frac{2v_{z,0}}{g}\sum_{i=1}^{k-1}\epsilon_z^{k-i} \end{aligned} \tag{16}$$

Since it is assumed that the ball has perfect grip on the field surface, the velocity of the contact point of the ball will be equal to the velocity of the surface after the first bounce. Therefore, the velocity components in horizontal directions remain constant after the first bounce. These velocities are dependent on the initial velocity and spin according to (13)-(14). Using this (16) can be rewritten as a function of the initial ball state only:

$$\begin{aligned} x(\tau,k,v_{x,0},v_{z,0}) = \\ &\frac{v_{x,0}+\alpha R_b\omega_{y,0}}{1+\alpha}\tau + \frac{2v_{z,0}v_{x,0}}{g} + \\ &\frac{2v_{z,0}(v_{x,0}+\alpha R_b\omega_{y,0})}{g(1+\alpha)}\sum_{i=1}^{k-1}\epsilon_z^{k-i} \\ y(\tau,k,v_{y,0},v_{z,0}) = \\ &\frac{v_{y,0}+\alpha R_b\omega_{x,0}}{1+\alpha}\tau + \frac{2v_{z,0}v_{y,0}}{g} + \\ &\frac{2v_{z,0}(v_{y,0}-\alpha R_b\omega_{x,0})}{g(1+\alpha)}\sum_{i=1}^{k-1}\epsilon_z^{k-i} \\ z(\tau,k,v_{z,0}) = v_{z,0}\epsilon_z^k\tau - \tfrac{1}{2}g\tau^2 \end{aligned} \tag{17}$$

From (17) it is clear that there are multiple initial ball states which result in a trajectory passing through the same target. There are three equations with eight parameters, namely six components of the initial ball state, time and a desired number of bounces. This provides extra freedom in choosing a correct and viable initial state. When the initial velocity and spin can be enforced on the ball independently of each other, extra information about the desired trajectory is necessary to get a single solution from (17) when solving for the initial state of the ball. It can for instance be desired to bounce at a certain location, or to pass through multiple targets throughout the path of the ball or to reach the target as fast as possible or with the lowest amount of spin. When the initial velocity and spin of the ball are coupled, it might be more difficult to set more requirements about the trajectory. When shooting the ball with the TURTLE, the latter case is true. Since the ball is kicked by applying a force in one direction, as will be explained in Section III-B, its initial velocity and spin direction are coupled. To find a viable initial state, this coupling has to be known. In the next section it is explained where this coupling comes from and how (17) can be used to determine the robot inputs to get as close to the target as possible.

III. Robot-Ball Interaction

In order to be able to enforce the desired initial state on the ball, it is first necessary to understand how the robot affects the ball prior to and during a shot. The interaction between the robot and the ball is modelled and tested. In Fig. 4 a schematic representation of this model is shown.

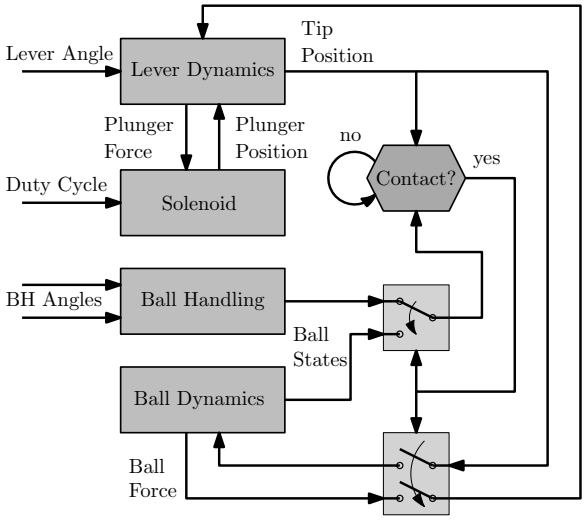

Fig. 4: Flowchart of the interaction between the robot and the ball. Prior to the shot, when the lever is not in contact with the ball, the ball states are determined by the ball handling system. When contact is made, its states are determined by the interaction between the ball and the lever, which is visualized by the switches.

From this figure it can be seen that there are four input settings which can affect the initial ball state. In this section these inputs and the sub-parts of this flowchart are explained. In Fig. 5 a picture of the TURTLE is shown. The ball handling mechanism and the shooting lever are clearly shown. The plunger is hidden behind the shooting lever.

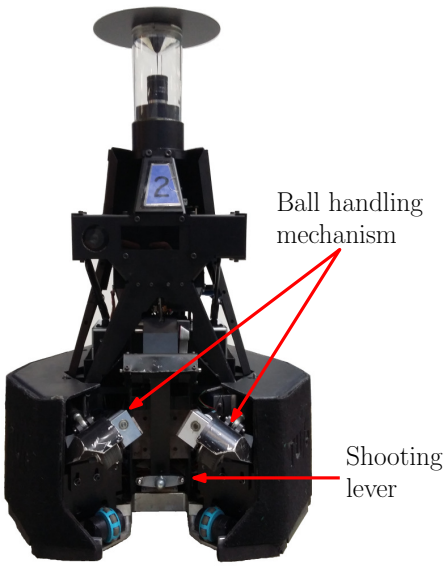

Fig. 5: Photograph of the front of the TURTLE as it was in July 2016. The solenoid is hidden behind the shooting lever.

A. Ball Handling

To control the ball, the TURTLEs are equipped with a ball-handling mechanism [15]. This mechanism consists of two levers, which are mounted on the front side of the robot. At the end of each lever a rubber wheel is attached which is able to rotate at a controlled speed to be able to control the ball. The levers are placed towards each other, under an angle of 30° with the y-direction and can rotate up and down around a hinge. The rotation of the levers is not actively controlled. When the robot is not in possession of a ball, the levers are in their lowest position. When the ball hits the wheels, they are actuated to contract the ball. During retraction, the levers will rotate upward to their highest position. The angles of the levers are measured using two potentiometers. Since the levers can pivot independently, the ball can be slightly shifted with respect to the robot without losing contact with the ball-handling wheels. By shifting the ball, the point of impact of the shooting lever is changed, which will be explained in Section III-C. This point of impact will have effect on the initial ball state.

It is assumed that the ball makes contact with the floor and both ball-handling wheels at any time during ball possession. Since the ball has three contact points, its position with respect to the robot can be estimated. For this estimation it is assumed that the ball and ball-handling wheels are spherical and have a fixed radius during contact. The position of the centre of each ball-handling wheel depends on fixed robot dimensions and the angle of the lever. When the centres of the ball-handling wheels are known, solving (18) for $\vec{r}_b$ provides the ball position.

$$\begin{aligned} |\vec{r}_b - \vec{r}_{w,l}| &= (R_b + R_w)^2 \\ |\vec{r}_b - \vec{r}_{w,r}| &= (R_b + R_w)^2 \\ r_{b,z} &= R_b \end{aligned} \tag{18}$$

Here, $\vec{r}_b$, $\vec{r}_{w,l}$, $\vec{r}_{w,r}$ are the position vector of the ball, left and right ball-handling wheel and R_w the radius of the ball-handling wheels respectively. Due to the assumption that the ball is not deformed by the ball handling wheels, the height of the ball's centre of mass is always equal to R_b. Experiments, that are explained in Appendix B, show that the relative position of the ball can be estimated with an accuracy of 0.63 mm and 1.34 mm in x- and y-direction respectively .

B. Shooting Lever

In order to shoot the ball, the robot is equipped with a mechanism, which exists of a high speed solenoid actuator and a shooting lever [16]. To power the actuator, energy is stored in a high voltage capacitor. By discharging this capacitor over the solenoid, a magnetic force propels a rod inside the solenoid, also called the plunger, forward. Using an IGBT, the energy through the solenoid, and thus the exerted force on the plunger, can be controlled. This is done by changing the duty cycle of a PWM signal which is used to switch the IGBT. The force on the plunger depends on the current flowing through the coil of the actuator and the inductance of this coil. The latter is a function of the position of the plunger, which makes the force on the plunger dependent on the position of the plunger.

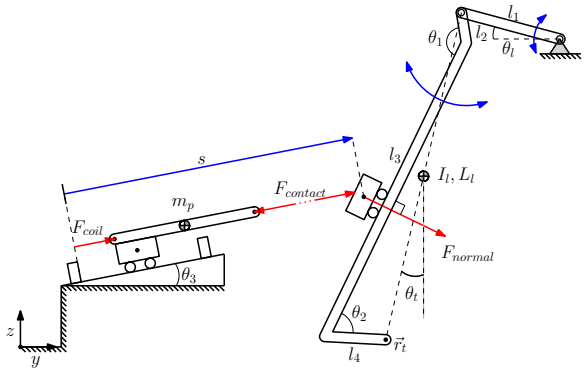

Fig. 6: Free body diagram of the shooting lever and plunger. The lever height can be set by rotating around the first hinge by an angle θ_l. The dimensions of the lever are given by $l_1 - l_4$, θ_1 and θ_2. The mass of the lever is represented by a point-mass at a distance l_l from the second hinge, with a mass moment of inertia of I_l, and θ_t the angle of the line that connects the tip of the lever with the second hinge with the z-axis. The plunger has a mass of m_p and moves in the s direction, with an angle of θ_3 with respect to the horizontal plane. F_{coil}, $F_{contact}$ and F_{normal} represent the magnetic force from the coil on the plunger, the contact force between the plunger and the lever, and the force perpendicular to the lever.

The tip of the plunger is fixed to the lever with a ball bearing to reduce friction between both parts. The bearing causes the force, exerted by the plunger on the lever, to only have a significant component perpendicular to the lever at the contact point. Because the plunger is fixed to the lever at all times, the position and velocity of the tip of the lever is a function of the position and velocity of the tip of the plunger. By solving a

force- and momentum equilibrium on the system as depicted in Fig. 6, an expression for the acceleration of the tip of the lever is found

$$\ddot{\vec{r}}_t = f(F_{coil}, s, \dot{s}, \theta_l) \tag{19}$$

where F_{coil} is the magnetic force exerted on the plunger, s is the position of the plunger in the direction of its motion and θ_l the angle of the part of the lever at the hinge with the horizontal plane. Due to the shape of the lever and the negligible low friction at the contact point with the plunger, the expression becomes non-linear. Several assumption have been made in the derivation of this expression; (1) all parts are infinitely stiff, (2) the tip of the lever only moves in the 2 dimensional vertical plane and the plunger only moves in one direction (s), and (3) friction between the plunger tip and lever, between the plunger and its casing, and in the hinges is negligible low.

C. Intrinsic Ball Dynamics

When the distance between the tip of the lever and the centre of the ball is at least R_b, contact is made. At this point, the force between the lever and surface of the ball will accelerate the ball. When the ball is hit off-centre, a force that is tangential to the balls surface will cause the ball to develop spin. In Fig. 7(a), a schematic representation of these forces is shown. To estimate these forces, the ball is modelled as a mass-spring-damper system

$$\begin{aligned} \vec{F}_b &= \Big(k_b\big(R_b - |\vec{n}_b|\big) - d_b\big(\dot{\vec{n}}_b \cdot \hat{\vec{n}}_b\big)\Big)\hat{\vec{n}}_b \\ \vec{n}_b &= \vec{r}_b - \vec{r}_t \\ \hat{\vec{n}}_b &= \tfrac{\vec{n}_b}{|\vec{n}_b|} \end{aligned} \tag{20}$$

where k_b, d_b and $\vec{r}_t$ are the spring and damper constant of the ball and the position of the tip of the lever respectively, and $\vec{n}_b$ the vector in the direction of the force. The tangential force is modelled as a friction force between the lever tip and the surface of the ball

$$\begin{aligned} \vec{F}_f &= \mu|\vec{F}_b|\hat{\vec{n}}_f \\ \vec{n}_f &= (\dot{\vec{r}}_t \times \vec{F}_b) \times \vec{F}_b \\ \hat{\vec{n}}_f &= \tfrac{\vec{n}_f}{|\vec{n}_f|} \end{aligned} \tag{21}$$

where μ is a friction coefficient and $\hat{\vec{n}}_f$ the direction vector of the friction force, which is assumed to be perpendicular to the ball radius at all times. The friction force will cause an angular acceleration, resulting in spin of the ball. The sum of both forces results in a net force which causes the ball to accelerate in the direction of this force.

Experiments have been conducted to get an indication of the intrinsic parameters of the ball, i.e. its spring- and damper constant. These experiments provide a direct measurement of the spring constant and an indirect measurement of the damper constant. An estimate of the damper constant is obtained through measuring the COR, which is described in Appendix C. In Appendix D a relation between the COR and the intrinsic ball properties is derived:

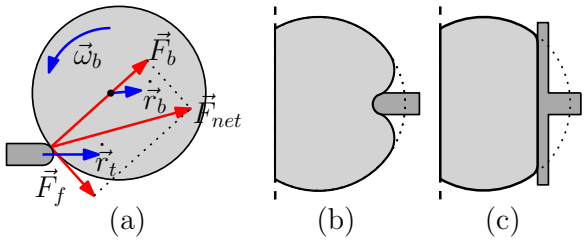

Fig. 7: Forces acting on the ball during the impact with the shooting lever (a). The size of the force between the ball and the impact tip depends on the area of the tip. A small area enables the ball to warp around the pin (b), minimizing the force, while a larger area prevents this (c).

$$\epsilon_z = \exp\left(\frac{-d_b\pi}{\sqrt{|d_b^2 - 4mk_b|}}\right) \tag{22}$$

When the mass, COR and spring constant of the ball is known, the damper constant can be estimated by solving (22) for d_b. The relation between the COR and the mass-, spring- and damper constant is based on the assumption that the ball is a weakly damped system, as is explained in Appendix D. From Fig. 20, Appendix C, it can be seen that the spring constant of the ball is linear and Fig. 8 shows that the spring constant is linearly dependent on the initial overpressure in the ball. Moreover, the spring constant depends on the indentation surface. When the ball is pressed with a small pin, the spring constant is lower than when it is pressed with a large plate. This is caused by the different modes of deformation of the ball. In the case of the small pin the ball can fold around the pin to minimize the impression volume, as is shown in Fig. 7, resulting in a lower force on the indentation pins. The ability to deform around the pin becomes smaller as the area of the pin becomes larger, which will cause the force to increase.

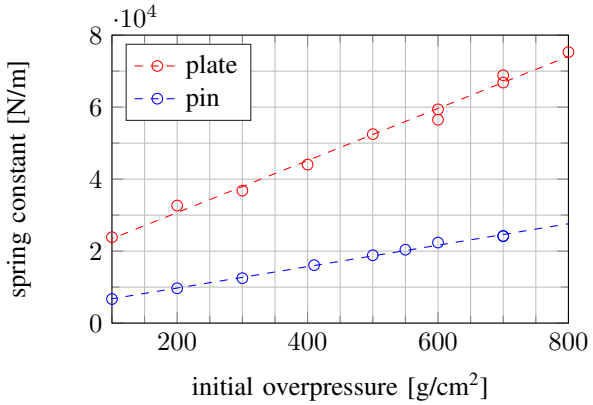

Fig. 8: The spring constant of the ball is shown for varying initial ball pressure, for both the indentation with a pin and a plate.

IV. Static Map for Input Selection

Using the model as discussed in Section III it is possible to determine the initial ball state ($\boldsymbol{q_0}$) for a given set of inputs to the robot ($\boldsymbol{u_r}$). However, in order to reach the target, the inverse problem should be solved; what inputs to the robot will lead to the desired initial ball state? Inverting the model of the robot-ball interaction could result in non-unique solutions, no solutions or solutions which cannot be achieved by the robot. It is necessary to determine reachable inputs at which the actual initial ball state is as close as possible to the desired ball states ($\boldsymbol{q_0^*}$), as discussed in Section II. These inputs can be found by solving a minimization problem

$$\arg\min_{\boldsymbol{u}_r \in \mathbb{U}} L\big(\boldsymbol{q_0^*}, m(\boldsymbol{u}_r)\big) \tag{23}$$

where $\mathbb{U}$ is the reachable input space, which is bounded by physical restriction of the hardware, and L the objective function which is based on the absolute difference between desired and estimated states or combination of states. In order to solve this problem, a static mapping function m is made, using the model, to estimate the initial ball state as a function of the robot inputs:

$$\tilde{\boldsymbol{q}}_0 = m(\boldsymbol{u}_r) \tag{24}$$

where $\tilde{\boldsymbol{q}}_0$ is an estimate of the initial ball state and $\boldsymbol{u}_r = [u_1, u_2, u_3, u_4]^T$ the input to the robot. The input contains the duty cycle to the IGBT of the solenoid, the angle of the shooting lever and the relative ball position with respect to the robot in both x- and y-direction respectively. The dynamics of the plunger, lever and ball during the interaction phase are captured in this map. This can be done under the assumption that the interaction is deterministic, i.e. the same set of inputs will always result in the same initial ball state. To get insight in what a good mapping function might be, an example of the effect of the robot inputs on the initial ball state is visualized in Fig. 9.

As a first approach, a polynomial function in two dimensions, u_1 and u_2, is used to approximate $v_{z,0}$. Increasing the degree of the polynomial will improve this approximation, but will also increase the complexity of the function, which is linked with the number of terms in the polynomial. A fourth order polynomial gives a fit with a coefficient of determination of $R^2 = 0.99$, which is an indicator that the fit describes the model well. The polynomial can be written as:

$$\tilde{\boldsymbol{q}}_0 = \boldsymbol{P}\boldsymbol{v} \tag{25}$$

where $\boldsymbol{P}$ holds the coefficients of the polynomials and $\boldsymbol{v}$ the non-linear combination of inputs u_1 and u_2. The constants in $\boldsymbol{P}$ only hold for one specific combination of u_3 and u_4, i.e. one relative initial position of the ball in x- and y-direction. When the ball is placed elsewhere, the coefficients in $\boldsymbol{P}$ might change. To account for this, another fourth polynomial relation is made between u_3 and u_4, and all coefficients $p_{i,j}$ in $\boldsymbol{P}$:

$$p_{i,j} = \boldsymbol{S}\boldsymbol{w} \tag{26}$$

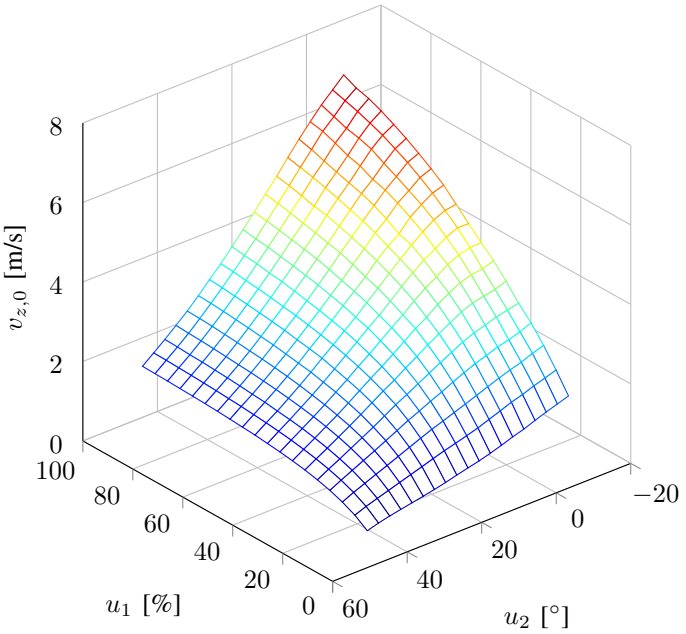

Fig. 9: Visualization of the effect of two robot inputs on one initial ball state. In this example initial position of the ball (u_3 and u_4) is kept constant and the duty cycle (u_1) and lever angle (u_2) are varied. The initial velocity of the ball in z-direction, as predicted from the interaction model, is shown.

where $\boldsymbol{S}$ holds the coefficients of this second polynomial and $\boldsymbol{w}$ the non-linear combination of inputs u_3 and u_4. By combining (25) and (26) the static map becomes a fourth order polynomial estimation in four dimensions.

V. Results

To test the free-motion model and the interaction model, two experiments are conducted. In this Section, these experiments and the results are discussed.

A. Validation of the Free-motion Model

To validate the free-motion model of a bouncing ball, the path of a ball is measured for different initial states. The set-up used to do this is described in Appendix A. The centre of the ball is tracked throughout its trajectory, from which its initial velocity is estimated. The initial spin is determined visually, making use of coloured marker stripes on the ball. The estimated initial velocity and spin are taken as input for the model in Fig. 3. The minimal distance between the measured and modelled position of the ball is defined as the absolute error. By doing so, the time at which the ball passes a certain point becomes irrelevant, as long as it passes the point. In Fig. 10 an example of the experiment is shown. The top figure shows the measured and modelled two dimensional position of the ball at equidistant times. The bottom figure shows the absolute error of the model as a function of the horizontal displacement of the ball. The ball properties and parameters used in the discrete state transition matrix (12) are given in Appendix A, Table II. In Fig. 11 the root mean square error (RMSE), over the entire measured trajectory, for different

initial velocities is shown. From this figure it can be seen that this error is below the radius of the ball for velocities up to 12 ms^{-1}. Therefore it is concluded that the model is sufficient in predicting the path of the ball.

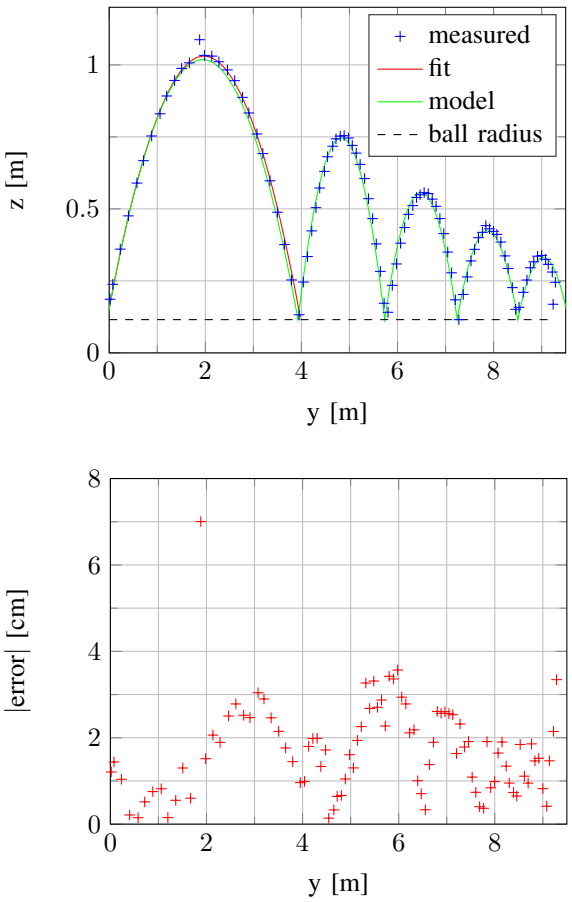

Fig. 10: Example of a conducted experiment with an initial velocity of 6.3 ms^{-1}. The top figure show the measured and modelled two dimensional position of the ball. The bottom figure show the absolute error, which is defined as the minimal distance between the measured and modelled position of the ball.

B. Validation of the Interaction Model

To validate the interaction model, it is preferred to test all sub-parts of this model, as discussed in Section III. This requires measurements of the velocities, accelerations and forces of the plunger, lever and ball during a shot. To do so, the robot and ball need to be equipped with numerous sensors. However, applying sensors to the plunger, lever and ball will change the dynamics of the systems, rendering the measurements useless to compare with the model. Instead, it is chosen to shoot at three targets of different heights, with the inputs to the hardware based on the model, and recording the position of impact of the ball with a camera. The robot will shoot at every one of these targets from four different distances. The height and distance of the targets are chosen to be directly reachable, i.e. the robot is able to hit

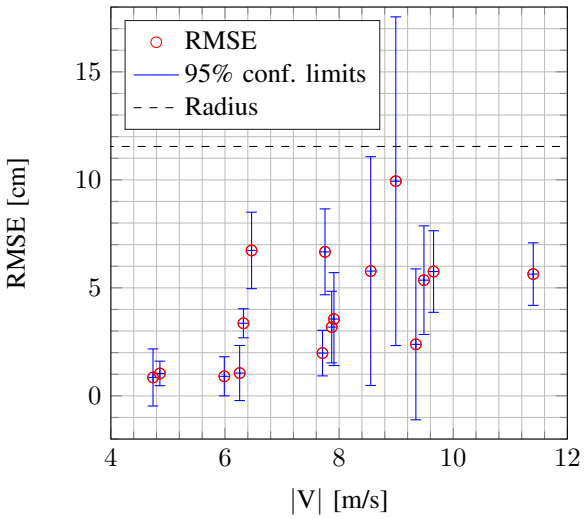

Fig. 11: Root mean square of the distance error for different initial ball velocities.

the targets from all chosen distances without exceeding the input space ($\boldsymbol{u}_r \in \mathbb{U}$) or the need of an intermediate bounce, and are placed in front of the robot in line with the y-axis. This simplifies the problem of solving (17) to solving (15b) and (15c). The desired initial velocity of the ball is found by setting $y(\tau)$ and $z(\tau)$ to the distance and height of the target, and $y_{\tau_0} = 0$ and solving for v_{y,τ_0} and v_{y,τ_0}. To be solvable, this approach needs one more requirement to account for the free variable τ. Therefore it is chosen to hit the targets with the top of the parabola ($\frac{dz}{d\tau} = 0$). If this is not possible, since the speed of the ball exceeds the maximal achievable speed, the shot angle is determined at which the ball can be shot with a speed of 10 ms^{-1} . This causes the ball to hit the target under a negative slope ($\frac{dz}{d\tau} < 0$). A bigger slope at the impact point will lead to larger deviation in case the positioning of the robot is not accurate. Before each shot the ball is fully retracted, causing the ball handling arms to be in their most upright position. This ensures that $\boldsymbol{P}$ in (25) is constant for each shot and that the problem is reversible; for each combination of v_{y,τ_0} and v_{z,τ_0} there is only one combination of duty cycle and lever angle. Directly inverting (25) is not possible since the elements in v are non-linear. Instead, a two fourth order polynomial, with the desired ball velocity as input, are used to estimate the duty cycle and lever angle. Every shot is repeated twenty times and the resulting impact locations of the ball are shown in Fig. 12.

A Gaussian distribution is assumed to be a sufficient approximation to describe the spread of the impact location. The mean impact location is shown in Fig. 12 and the covariance of the shot is visualised by an ellipse [17]. It can be seen that for most shots there is a bias above and left from the target. This bias is produced by system- and model errors. For instance, the angle of the lever at the time of the shot differs from the desired angle due to bad controller performance. Also, the voltage over the capacitor varies between shots, causing the effective magnetic force acting on the plunger to vary with it.

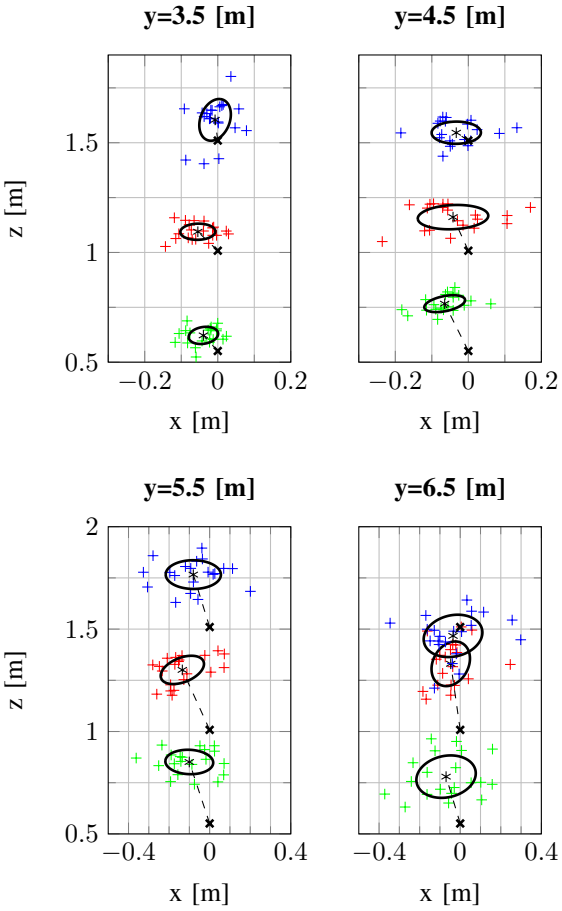

Fig. 12: Impact locations of the ball on the plate in x- and z-direction for several distances y to the plate. The cross marks a target, the plus marks an impact location, the star marks the mean impact location and the ellipse represent on standard deviation from the mean for every shot taken.

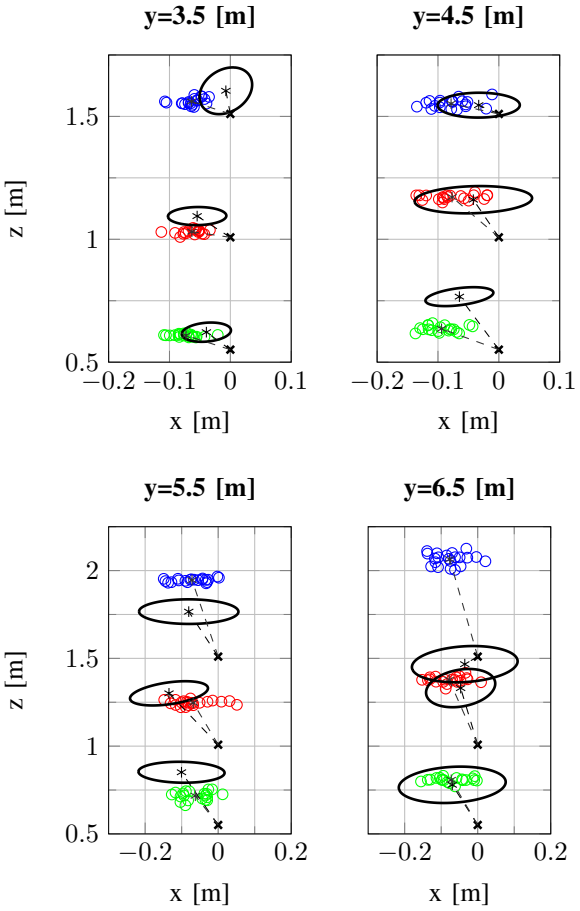

Fig. 13: Prediction of the impact points where the robot settings, measured during the experiments, are taken as inputs to the model. The mean and standard deviation of the measured shots are shown to get a sense of the correctness of the model.

The actual settings of the robot during the shot are used as inputs to the model. This gives a new prediction of where the ball would hit the plate according to the model. The difference between this model based impact prediction and the actual impact position gives a sense of the model error. In Fig. 13 the predicted impact locations, with the measured robot inputs, and the mean and deviation ellipses of the real impact locations are shown.

It can be seen that there is still a discrepancy between the locations. The difference between the predicted and actual impact location can be caused by non-modelled dynamics, such as the effect of the ball handling wheels on the initial ball state. Another cause is the estimation of the actual position of the ball on the field, and thus the distance to the target, which has a limited accuracy. The difference between the mean of the measured impact positions and the mean of the predicted impact positions in both directions are given in Table I. From this table it can be seen that the impact point can be predicted with an accuracy lower than the ball diameter, with the exception of one outlier.

TABLE I: Difference between the means of the measured- and predicted impact positions in two directions (in centimetres). The distance and height of the corresponding targets is given.

Distance to target [m]	**Height of target [m]**		
	0.551	**1.008**	**1.510**
3.5	x = 3.34 z = 1.35	x = 0.87 z = 6.36	x = 5.63 z = 4.32
4.5	x = 2.93 z = 13.08	x = 3.49 z = -1.06	x = 4.54 z = -0.67
5.5	x = -3.78 z = 13.39	x = -6.63 z = 5.37	x = -0.90 z = -17.93
6.5	x = 0.28 z = -2.85	x = 3.15 z = -4.70	x = 4.13 z = -59.83

VI. Conclusions and Recommendations

A model that describes the path of a bouncing ball is created and validated. When the initial state of the ball is known, this model can predict its path with an accuracy in the order of the ball radius. This implies that the requirement of hitting a target with an accuracy of at least one times the ball diameters is met if the correct initial ball states can be achieved. The robot has four inputs which affect the state of the ball during the shot. A model is created which estimates the initial state of the ball as a function of the robot inputs. This model is used to determine the robot inputs, which correspond to the desired initial ball state, in order to hit several targets. Experiments show that there is a significant offset between the targets and the actual impact position. This is mainly due to controller limitations of the lever, resulting in an error between the desired- and actual lever position, and a variation in the voltage over the capacitor. A prediction of the impact points based on the measured robot inputs shows that most impact positions can be estimated with an accuracy lower than the ball diameter. The difference between the predicted and actual impact location suggests that some dynamics is not modelled, for instance the effect of the ball handling on the ball during the shot.

In the future, when the robots are able to achieve higher ball velocities, the model of the path of the ball must be extended by incorporating aerodynamic effect during flight. Also, when playing on a slippery field, possible slip during the bounce needs to be investigated. To understand which parts of the interaction model are correct and which need improvements, the sub-parts of the model need to be tested. Moreover, the forces between the ball handling wheels and the ball need to be incorporated into the model. More research should be done on to see whether the correlation between the COR and the spring- and damper constant of the ball is valid, for instance by also directly measuring the damping constant of the ball. Instead of using a polynomial fit to estimate the robot inputs corresponding to the desired initial ball state, other approaches might be investigated to see if the shots can be improved. The biggest improvement in order to hit a target can be made by improving the performance of the lever controller and a better estimation of the force on the plunger as a function of the voltage over the capacitor. These improvements will lead to a better match between the desired initial state of the ball and its actual state.

References

[1] J. W. M. Bush, "The aerodynamics of the beautiful game," in *Sports Physics*. Les Editions de l'Ecole Polytechnique, 2013, pp. 171–192.

[2] G. Dupeux, C. Cohen, A. Le Goff, D. Quéré, and C. Clanet, "Football curves," *Journal of Fluids and Structures*, vol. 27, pp. 659–667, 2011.

[3] A. M. Nathan, "The effect of spin on the flight of a baseball," *American Journal of Physics*, vol. 76, no. 2, p. 119, 2008.

[4] R. Cross, "The coefficient of restitution for collisions of happy balls, unhappy balls, and tennis balls," *American Journal of Physics*, vol. 68, no. 11, pp. 1025–1031, 2000.

[5] ——, "Grip-slip behavior of a bouncing ball," *American Journal of Physics*, vol. 70, no. 11, p. 1093, 2002.

[6] ——, "Bounce of a spinning ball near normal incidence," *American Journal of Physics*, vol. 73, no. 10, p. 914, 2005.

[7] R. Cross and A. M. Nathan, "Experimental study of the gear effect in ball collisions," *American Journal of Physics*, vol. 75, no. 7, p. 658, 2007.

[8] R. Cross, "Impact of a ball on a surface with tangential compliance," *American Journal of Physics*, vol. 78, no. 7, p. 716, 2010.

[9] J. Y. Choi, B. R. So, and W. Kim, "Impact based trajectory planning of a soccer ball in a kicking robot," in *Proceedings of the 2005 IEEE International Conference on Robotics and Automation*, no. April, Barcelona, Spain, 2005, pp. 2845–2851.

[10] R. Cisneros, K. Yokoi, and E. Yoshida, "Impulsive pedipulation of a spherical object for reaching a 3d goal position," in *International Conference on Humanoid robots (Humanoids)*, 2013, pp. 154–160.

[11] D. Alain, "Perfecting of a ball bounce and trajectories simulation software: In order to predict the consequences of changing table tennis rules," *International Journal of Table Tennis Sciences*, vol. 2, pp. 15–32, 1994.

[12] W. Stronge and A. Ashcroft, "Oblique impact of inflated balls at large deflections," *International Journal of Impact Engineering*, vol. 34, no. 6, pp. 1003–1019, jun 2007.

[13] R. Cross, "The bounce of a ball," *American Journal of Physics*, vol. 67, no. 3, pp. 222–227, 1998.

[14] M. Heemels and B. d. Schutter, "Lecture notes on modeling and control of hybrid dynamical systems," Department of Mechanical Engineering, Eindhoven University of Technology, pp. 11–13, November 2013.

[15] J. de Best and R. van de Molengraft, "An active ball handling mechanism for robocup," *2008 10th International Conference on Control, Automation, Robotics and Vision*, pp. 2060–2065, dec 2008.

[16] K. J. Meessen, J. J. H. Paulides, and E. a. Lomonova, "A football kicking high speed actuator for a mobile robotic application," *IECON 2010 - 36th Annual Conference on IEEE Industrial Electronics Society*, pp. 1659–1664, nov 2010.

[17] M. Ribeiro, "Gaussian probability density functions: Properties and error characterization," *Institute for Systems and Robotics, Technical Report*, no. February, pp. 1–30, 2004.

APPENDIX A
FREE FLIGHT TEST SETUP

To verify the free flight model, the path of a ball is measured for a number of different initial states. In order to do this in a controlled way, a fifth edition TURTLE robot[2] is used to do the shooting.. The robot uses a shooting lever to create an impact on the ball. This lever is activated by a high speed reluctance actuator [16] and can be lowered to hit the ball beneath its centre of mass, which enables the robot to give lob shots. To alter the lever speed, the voltage over the actuator can be controlled using a PWM signal. By changing the lever position and actuator speed, the initial states the ball can be changed. For the conducted experiments the lever is kept in its lowest position, the duty cycle of the PWM signal is altered to get different ball velocities.

The experiments are done on the training field of robot football team TechUnited in Eindhoven. This field measures 12x8 meters and is made to resemble a part of a standard MSL football field, including two goals. The surface of the field is made of low pile carpet material. The field lines are painted onto the surface. Because the lines have a different surface texture, the ball might interact differently with the lines than with the carpet. Therefore the robot is placed in a corner next to the field for these experiments. This way the ball can travel a distance of more than twelve meter without hitting any field lines. In Fig. (14) a schematic representation is made of the test set-up. Parallel to the plane of motion, at a distance of approximately 0.3 meters, four reference markers are added to the background, as can be seen in Fig. (15). Connecting these markers will result in a square. The edges of this square are used as a reference to set up the camera as straight as possible and the distance between the markers are used as a scale of reference. In Fig. (15) it can also be seen that there is a length scale present. This scale is made from differently coloured squares with a length of 10 cm and is used as a visual reference.

To track the course of the ball, a CASIO EX-F1 camera is placed next to the field. When the camera is placed further away from the plane of motion of the ball, more of its trajectory can be seen. However, the ball will become smaller in the taken images, making image analyses difficult. Therefore, there is a trade-of concerning the placement of the camera. It is chosen to place the camera at a distance of twelve meters from the plane of motion of the ball. At this distance approximately nine meters of the horizontal displacement of the ball can be tracked, while still getting an image of the ball that is clear. The clarity of the ball is linked to the number of pixel used to display the ball in the images. Being able to film a clear ball is necessary since the processing of the images, and thus the tracking, will be done automatically. An algorithm is developed using Matlab to process the videos from the experiments. In order to determine the angular velocity of the ball, three different coloured stripes are applied to the surface of a white ball using permanent markers. With these marker lines the spin of the ball is determined visually from the footage. The properties of test-ball are given in Table (II).

[2]http://www.roboticopenplatform.org/wiki/

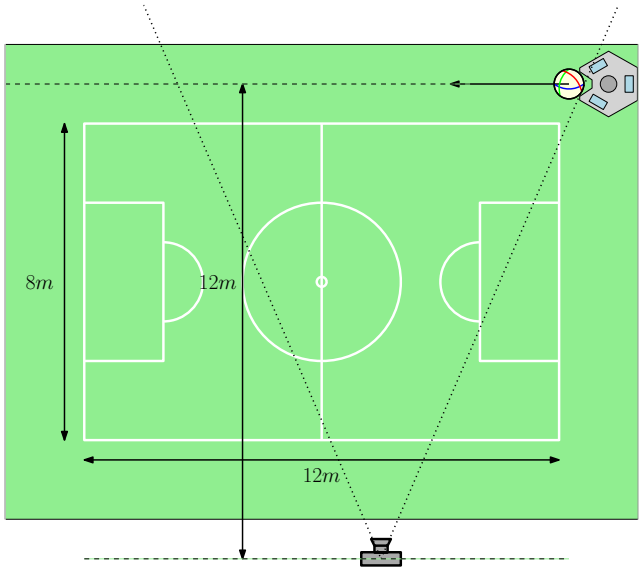

Fig. 14: A schematic representation of a to view of the test set-up.

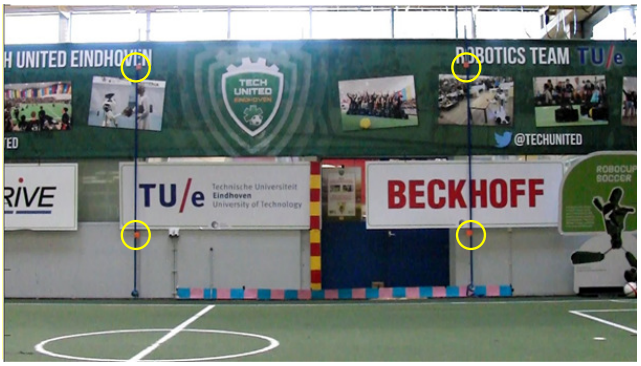

Fig. 15: Background including reference markers (encircled) and length scale.

TABLE II: Properties of the used test ball

Property	Symbol	Value	Unit
Mass	m	433.6	g
Circumference	s_b	72.5	cm
Radius	R_b	11.55	cm
Pressure	P_{ball}	0.6 58 839.9	kg/cm^2 Pa
COR	ε_z	0.84	–
Correction factor	α	0.83	–

APPENDIX B
BALL HANDLING TEST SETUP

Because the relative position of the balls centre of mass cannot be measured directly, it needs to be determined indirectly. In Section III-A this is already explained. Solving (18) should give an estimation of the relative ball position. In order to verify this, experiments are conducted. First, a relation between the potentiometers and the actual angle of the ball handling levers is determined. This is done by fixing the levers in several positions, measuring their angle w.r.t. the horizontal plane with an inclinometer and reading out the output voltage of the potentiometer. From Fig. 16 it can be seen that the relation between the output voltage and lever angles can be described by a linear function. It can also be seen that the range of the angles and voltages for both levers are different. To get a quick estimate of the linear relation, the angles and voltages of both levers need to be measured at at least two different positions.

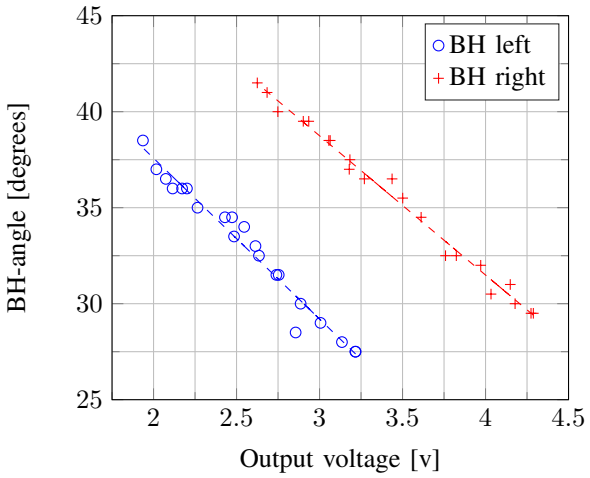

Fig. 16: Angles of both ball handling levers as a function of the output voltage of the potentiometers.

Now that the angles of the levers can be estimated through measuring the voltages of the potentiometers, $\vec{r}_{w,l}$ and $\vec{r}_{w,r}$ can be calculated and (18) can be solved for $\vec{r}_b$. To check the correctness of this estimated relative ball position, the actual position of the ball w.r.t. the robots centre is measured. To do this, the robot with ball is placed onto a glass table. A camera is placed beneath the table to capture pictures from the bottom of the robot and ball. In order to determine the contact point of the ball with the table, blue LED light is added to the side of the glass plate. This light shines into the plate and will light up any object that is placed onto the table, in this case the ball. From Fig. 17 it can be seen that the contact point of the ball with table indeed lights up. This point is not necessarily the centre of the yellow blob that is the ball because the camera is centred underneath the robot and not the ball.

Two perpendicularly placed measuring tapes are used to determine the relative distance between the robots centre and the contact point of the ball in the horizontal plane. This distance is measured for several different angles of the ball handling levers. The predicted and measured values for the relative x and y-position of the ball are shown in Fig. 18. From this figure it can be seen that the predictions by solving (18) are accurate. When taking the RMS of the absolute error between the measured and predicted values in both directions, this amounts to a prediction error of 0.63 mm and 1.34 mm in x- and y-direction respectively.

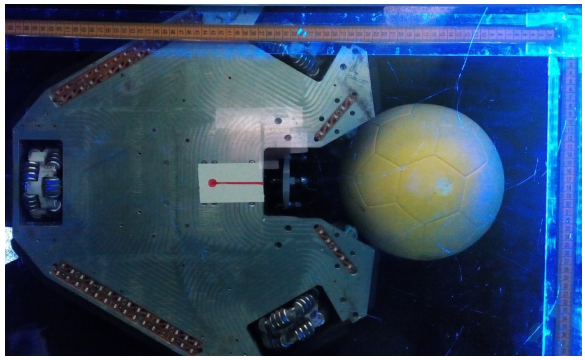

Fig. 17: Picture taken from underneath the robot while handling the ball. The centre and direction of the robot is visible in red. The contact point of the ball with the table is accentuated by the blue LED light.

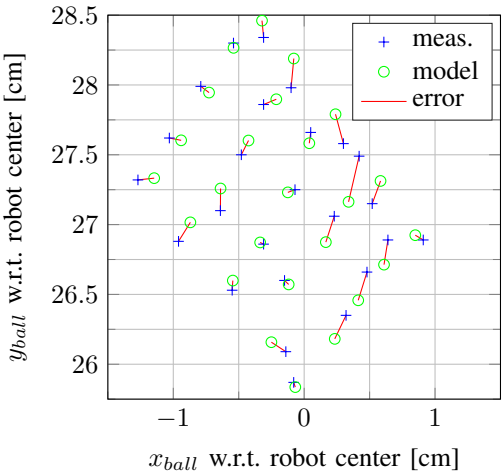

Fig. 18: Relative ball position of the ball w.r.t. the robots centre in the horizontal plane.

APPENDIX C
INTRINSIC BALL DYNAMICS TEST SETUP

To estimate the forces between the tip of the lever and the ball during the kick, the ball is modelled as a mass spring damper system. The ball can be seen as a flexible shell which is attached to a point-mass, in the centre of the shell, by an infinite amount of parallel springs and dampers. When the ball is impacted, the shell will be pressed towards the centre of mass. At the point where the shell is deflected, the springs and dampers will result in a force which will cause the mass to move. To simplify the estimation of the force, the vast amount of active springs and dampers are substituted by one substitute spring and damper. The behaviour of these substitutes might depend on the shape and amount of the indentation. To test the behaviour of the substitute spring and damper, indentation tests are done. The test set-up is shown in Fig. 19.

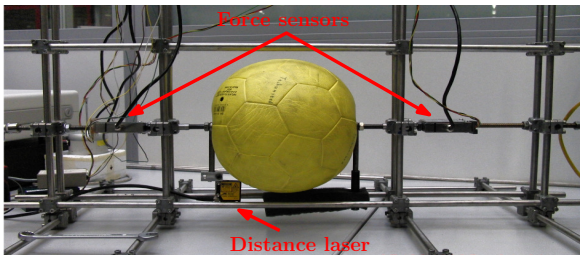

Fig. 19: Picture from the measurement set-up. The ball is clamped between two indentation rods. The force exerted on the ball is measured with two force sensors in the rods, one on either side. The relative distance between the rods is measured with the laser underneath the ball.

The ball is placed freely between two indentation rods, which are positioned opposite and parallel with each other. The centre of mass of the ball is positioned on the working line between the rods. When the rods are slowly moved towards the centre of the ball, the shell of the ball will deform symmetrically. The force exerted on both rods and the distance between them can be measured, which gives a measure for the spring constant. To measure the forces two KAP-E/D force transducers are incorporated into both rods. The distance is measured with a Baumer OADM 12U laser sensor which is attached between the rods. The data acquisition is done by a DAQ system and software developed by the TU/e. The indentation tips on the rods can be changed to test different indentation areas. Two sets of measurements have been done; one with a small indentation tip and one with a large plate pressing onto the ball. In Fig. 20 the sum of the forces is shown as a function of the indentation distance. This is done for several different initial ball pressures to see the effect of the initial pressure on the spring constant.

From Fig. 20 it can be seen that for all initial pressures, the relation between the sum of force and the indentation is linear. The measurements with the small tip resulted in a similar relation. The spring constant of one spring is twice the value of the measured slope, since the springs are placed serial. The effect of the initial ball pressure on the spring constant is seen in Fig. 8. From this figure it can be seen that this relation is

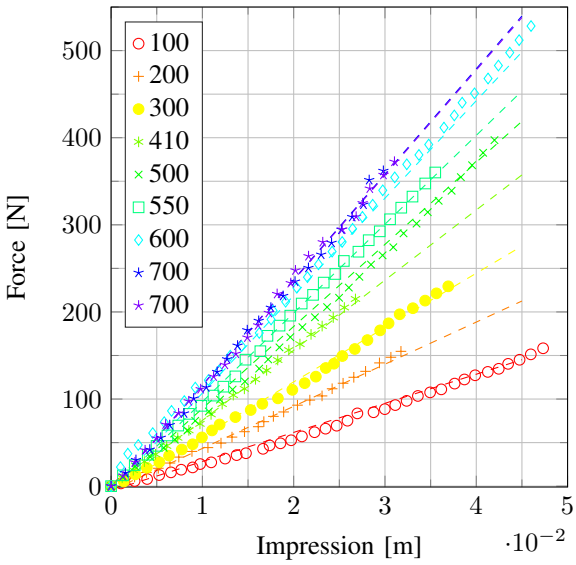

Fig. 20: Impression measurements on the ball; the combined forces are shown as a function of the indentation for several initial ball pressures (in g/cm^2), impressing the ball with a large area plate.

also linear. It also shows that the spring constant is higher for the larger indentation area.

A relation for the dampers could be found in a similar fashion, by applying an alternating force and measuring the speed of the indentation. Due to limitation on the set-up and DAQ system, this is not possible. The damper constant is estimated by using the relation between the intrinsic ball properties and its COR, as is discussed in Appendix D. Since the spring constant is known and the mass of the ball can be measured, the damping can be estimated by measuring the COR of the ball and solving (22). To do so, the ball is filmed while bouncing from a height of approximately 2 meter onto a solid concrete floor. The centre of the ball is tracked in similar fashion as is discussed in Appendix A. By comparing successive bouncing heights, the COR can be determined with (2). This experiment is done for several different initial ball pressures. In Fig. 21 the result of these experiments is shown. Since the impact on the floor is comparable to indentation with a large area, the spring constant of the measurement with the large plate is used in combination with the COR to find a value for the damper. This is done for all tested initial ball pressures and can be seen in Fig. 22. The damping constant appears to be constant for all initial ball pressures. It is believed that the damping is a result of the friction between the fibres of the shell material of the ball during deformation. The shape of this deformation is dependent on the impressing surface. When impressing the ball with a large area, the shape of the deformation is roughly the same regardless of the initial ball pressure. This explains why the damping constant is the same for all initial ball pressures when being impressed with a large area. Measuring the damping constant indirectly is only done for the flat plate indentation because getting good measurements of the COR for the pin indentation is not possible. It is assumed that the damping constant for the

pin indentation will be lower than the damping constant for the plate indentation, analogous to the spring constant. It is also believed that the damping constant for the pin indentation might not be constant for all initial ball pressures. The shape of the deformation of the shell of the ball varies with the initial ball pressure.

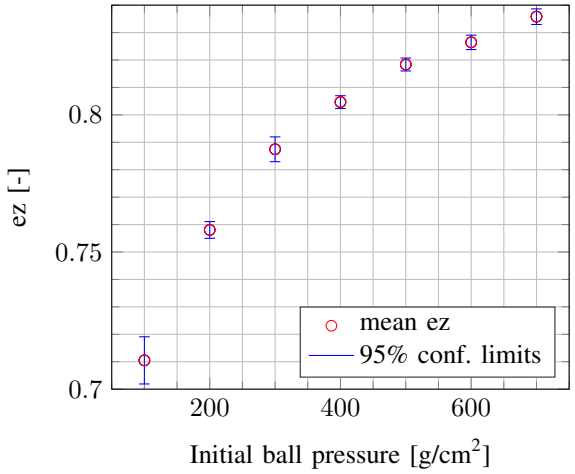

Fig. 21: The coefficient of restitution of the ball as a function of the initial ball pressure.

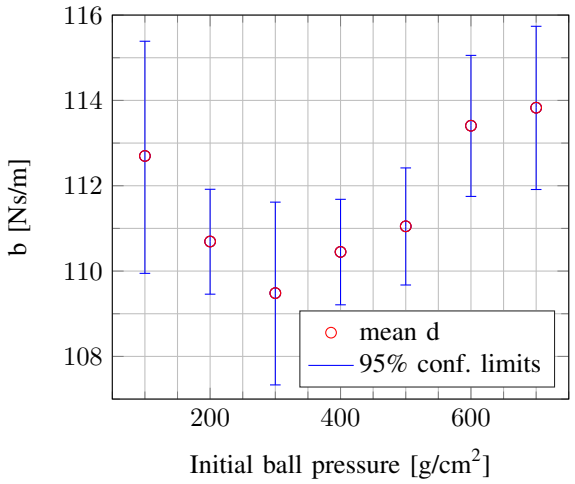

Fig. 22: The damping constant of the ball as a function of the initial ball pressure.

APPENDIX D
COEFFICIENT OF RESTITUTION AS A FUNCTION OF INTRINSIC BALL PROPERTIES

Conventionally, the energy loss during a bounce of the ball is accounted for by the coefficient of restitution. By modelling the intrinsic ball dynamics by a mass-spring-damper system, a relation between the COR and the intrinsic constants can be found. When the shell of the ball touches the surface the system can be described as a mass which is connected to the solid floor with a spring and a damper, as is shown in Fig. 23.

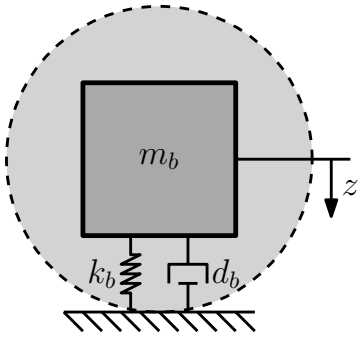

Fig. 23: The moment at which the shell of the ball hits the solid floor, it can be described by a mass-spring-damper system with $z_0 = 0$ and $\dot{z}_0 = v_z^-$

The equation of motion of this system is given by (27), with initial condition $z_0 = 0$ and $\dot{z}_0 = v_z^-$.

$$m\ddot{z} + d_b\dot{z} + k_b z = 0 \tag{27}$$

When the ball strikes the ground with a significant velocity, it will bounce back after impact. This observation leads to the assumption that the ball is an under-damped system; $d_b^2 < 4mk_b$. The roots of (27) are complex and the general solution becomes

$$\begin{aligned} z(t) &= c_1 e^{-at} cos(\omega_d t) + c_2 e^{-at} sin(\omega_d t) \\ \text{with} \quad \omega_d &= \tfrac{\sqrt{|d_b^2 - 4mk_b|}}{2m} \quad \text{and} \quad a = \tfrac{d_b}{2m} \end{aligned} \tag{28}$$

where ω_d is the damped frequency of the system. Using the initial condition a closed form solution of the position and velocity of the centre of the ball is found.

$$z(t) = \frac{v_z^-}{\omega_d} e^{-at} sin(\omega_d t) \tag{29}$$

$$\dot{z}(t) = v_z^- \Big(cos(\omega_d t) - \frac{a}{\omega_d} sin(\omega_d t) \Big) e^{-at} \tag{30}$$

The centre of the ball will initially move towards the floor, stop at some time and back upward. The spring and damper are not fixed to the floor. Therefore, when the centre of ball reaches its initial for the first time again, it is assumed that there is no contact with the floor any more. The time at which this happens is found from (29) and results in $t^+ = \pi\omega_d^{-1}$. The velocity at this time is found by solving $v_z^+ = \dot{z}(t^+)$.

$$v_z^+ = -\exp\left(\frac{-a\pi}{\omega_d}\right) v_z^- \tag{31}$$

Combining (31) with (2) gives an expression for the COR

$$\epsilon_z = \exp\left(\frac{-a\pi}{\omega_d}\right) = \exp\left(\frac{-d_b\pi}{\sqrt{|d_b^2 - 4mk_b|}}\right) \tag{32}$$